International Journal of Heat and Fluid Flow 29 (2008) 1447–1455

Contents lists available at ScienceDirect

International Journal of Heat and Fluid Flow

journal homepage: www.elsevier.com/locate/ijhff

Numerical simulation of fluid flow in microporous media

Rui-Na Xu [a,b], Pei-Xue Jiang [a,*]

[a] Key Laboratory for Thermal Science and Power Engineering of Ministry of Education, Department of Thermal Engineering, Tsinghua University, Beijing 100084, China
[b] Institute of Nuclear and New Energy Technology, Tsinghua University, Beijing 100084, China

ARTICLE INFO

Article history:
Received 8 November 2007
Received in revised form 1 April 2008
Accepted 13 May 2008
Available online 9 July 2008

Keywords:
Fluid flow
Microporous media
Slip flow
Numerical simulation

ABSTRACT

The flow characteristics of water and air in microporous media with average diameters of 200 μm, 125 μm, 90 μm, 40 μm, 20 μm, and 10 μm were studied numerically. The calculated friction factors for water and air in the non-slip-flow regime in the microporous media agree well with the known correlation suitable for normal size porous media. The numerically predicted friction factors for air in the slip-flow regime in the microporous media with 90 μm, 40 μm, 20 μm, and 10 μm diameter particles were less than the correlation for normal size porous media but close to experimental data and a modified correlation that accounts for rarefaction. Comparisons of the numerical results with the experimental data and the modified correlations show that rarefaction effects occur in air flows in the microporous media with particle diameters less than 90 μm and that the numerical calculations with velocity slip on the boundary can properly simulate the fluid flow in microporous media.

1. Introduction

Fluid flow and convection heat transfer in porous media have received much attention for many years due to their importance in many applications such as electronic equipment cooling, transpiration cooling, hydrogen storage, packed bed regenerators, combustors, micro thrusters, catalysis, adsorption, fuel cells, oil extraction, fixed bed reactors, disposal of hazardous waste, and various chemical processes. In recent decades there have been many experimental and numerical investigations of fluid flow and convection heat transfer in sintered porous media and non-sintered packed beds with normal size particles, such as Vafai and Tien (1981), Wakao and Kaguei (1982), Hsu and Cheng (1990), Amiri et al. (1995), Quintard (1998), Jiang et al., (1999a, 1999b, 2001, 2004, 2006a), Alazmi and Vafai (2002) and Tzeng et al. (2006). Fluid flow through porous media is usually modeled using a volume-averaged approach. Darcy's law is valid for fluid flows with Reynolds numbers less than one. The Ergun equation based on experimental data is often used for higher Reynolds numbers (Ergun, 1952). Correlations of the friction characteristics based on experimental results have also been developed (Aerov and Tojec, 1968). Ma et al. (2006) explored the flow resistance and forced convective heat transfer effects for three types of flow orientations in a packed channel. Their investigations established a series of empirical correlations for the three flow orientations and d_p = 3–6 mm.

Fluid flow in microporous media also has significant scientific and practical importance in many areas. For transpiration cooling of walls exposed to high heat fluxes, the particle diameters in the porous walls are usually 1–30 μm. For hydrogen storage, the particle diameters in the porous hydrogen storage alloys are 1–20 μm. Better knowledge about the fluid flow characteristics and improved heat and mass transfer models for microporous media are very important for the development of transpiration cooling, hydrogen storage and other related technologies. There have been a number of studies on the phenomenon of fluid flow through microporous media. Scheidegger (1974) introduced the physics of flow in porous media and gave a detailed review of the pioneering theories and investigations. In recent years, the theory of gas transport through microporous media has been studied extensively by various researchers, such as Kast and Hohenthanner (2000), Pavan and Oxarango (2007), Bravo (2007), and Miguel and Serrenho (2007). A number of studies have found that for the same porous media the permeability with gases is larger than with liquids and the permeability differs with different gases (Klinkenberg, 1941; Scheidegger, 1974; Miguel and Serrenho, 2007). According to Klinkenberg (1941), this phenomenon may be attributed to slip when gas flows in the microporous media (Miguel and Serrenho, 2007). The Knudsen number, Kn, the ratio of the mean free path of the gas to the pore diameter (Kast and Hohenthanner, 2000), classifies the gas flow into four flow regimes: the continuum flow regime (Kn < 0.001), the slip flow regime (0.001 < Kn < 0.1), the transition flow regime (0.1 < Kn < 10) and the free molecular flow regime (Kn > 10). Jones and Owens (1980), Sampath and Keighin (1982) and Ertekin et al. (1986) investigated gas slippage in tightly packed sands. The porosities of their test sections were less than 15%. They

* Corresponding author. Tel.: +86 10 62772661; fax: +86 10 62770209.
E-mail address: Jiangpx@mail.tsinghua.edu.cn (P.-X. Jiang).

0142-727X/$ - see front matter © 2008 Elsevier Inc. All rights reserved.
doi:10.1016/j.ijheatfluidflow.2008.05.005

Nomenclature

d_h	average pore diameter (=$2d_p\varepsilon/(3(1-\varepsilon))$), m
d_p	particle diameter, m
f_e	friction factor
F	inertia coefficient
l	average molecular free path, m
L	test section length, m
k_B	Boltzmann constant (1.38066×10^{-23} J/K)
K	porous medium permeability (m^2)
Kn	Knudsen number (=l/d_h)
M	Mass flux (=ρu), kg/(m^2s)
P	pressure (Pa)
Re_e	equivalent Reynolds number (=$2Md_p/(3\mu(1-\varepsilon))$)
u	velocity, m/s
U	non-dimensional velocity components parallel to the wall
V	non-dimensional velocity components normal to the wall
x, y, z	coordinates, m

Greek letters

δ	distance from cell-center to the wall, m
α_v	momentum accommodation coefficient of the gas (assumed to be 0.6)
σ	Lennard–Jones characteristic length
ε	porosity

Subscripts

0	test section inlet
g	gas
w	wall
c	cell-center

found that gas flow through the microscale and nanoscale pore structures may fall into the slip or transition regime.

In spite of the many studies of fluid flow in porous media, the flow mechanisms in microporous media still need to be investigated further. The Klinkenberg effect and the influence of slip flow on the permeability at low velocities were mainly studied. However, in some practical applications such as transpiration cooling, the gas velocities in the microporous wall are quite high and the inertia effect can not be ignored. For this case, the Brinkman-Darcy-Forchheimer model needs to be used to describe the fluid flow in the microporous media. In this model, the inertia coefficient, F, is also an important parameter along with the permeability K. The influence of the slip flow on the inertia coefficient, F, in microporous media needs to be studied; however, the very few investigations of high velocity fluid flow in microporous media did not discuss the influence of compressibility, rarefaction and particle or pore size on the fluid flow (Polyaev et al., 1996, Antohe et al., 1997), so no modified models for F in microporous media can be found in the literature. Thus, new models including the effects of compressibility and rarefaction for K and F are needed to accurately simulate the fluid flow and heat transfer in microporous media.

In recent years, particle-level numerical simulations have been used to study single-phase fluid flow and convection heat transfer in porous media (Logtenberg et al., 1999; Nijemeisland and Dixon, 2001; Nijemeislanda et al., 2004; Jiang and Lu, 2006a). Nijemeisland and Dixon (2001) gave a review of earlier works on discrete particle simulations of flows in fixed beds. Magnico (2003) studied the flow around packed spheres in a cylindrical container with pore scale flow simulations. Nijemeisland and Dixon (2001) studied the detailed velocity and temperature fields and the relationship between the local flow field and the local wall heat flux in a packed bed of spheres based on particle-level numerical simulations. Guardo et al. (2005) also used computational fluid dynamics to obtain a more detailed view of the fluid flow and heat transfer mechanisms in fixed bed reactors. Jiang and Lu (2006a) showed that the fluid flow and convective heat transfer rates of water in sintered bronze porous plate channels predicted using particle-level numerical simulations agreed well with well-known correlations. Jiang et al. (2006b) presented three-dimensional numerical simulations using the CFD code FLUENT to predict the particle-to-fluid heat transfer coefficients and to provide details of the fluid flow inside the miniporous media.

There is strong evidence to support the use of continuum momentum and energy equations to model slip flow, with the boundary conditions appropriately modified by imposing velocity slips and temperature jumps at the walls (Eckert and Drake, 1972). Liu et al. (1995) showed that the Navier-Stokes equations combined with slip flow conditions could represent experimental data in some microchannel flows. In recent years, the velocity slip conditions with second-order Knudsen number effects have been used to take into account the rarefication effects in moderately rarefied flows. Maurer et al. (2003) showed that second-order models can be extended to an outlet Knudsen number of 1.46, provided the second-order coefficient is suitably calibrated to fit the experimental data.

Xu et al. (2008) experimentally studied the flow characteristics of water, air, helium and hydrogen in microporous tubes with average diameters of 10–225 μm. The experimentally measured friction factors for water in the porous media with diameters of 200 μm and 40 μm agreed well with the known correlation. However, the compressibility significantly influenced the gas flow in micro porous media with particle diameters of 10 μm–200 μm. The experimental results show that evident rarefaction effects occur in air flows in the microporous media with particle diameters less than 90 μm.

The present paper numerically investigates water and air flow in micro porous media with average diameters of 10–200 μm. The numerical simulation results are compared with experimental data to provide details of the fluid flow inside the microporous media. The air flow characteristics in the microporous media are investigated for various particle diameters and Knudsen numbers. The aim of this paper is to further explore the mechanism of flow characteristics through microporous media and to prove that the slip flow on the solid surface is the reason for the decrease of friction factor or increase of the permeability in microporous media. In addition, the particle-level numerical simulation with the slip flow boundary conditions for the slip flow regime can be proved to be a useful method to investigate the flow characteristics in the microporous media.

2. Physical model, governing equations and numerical method

The friction factors in the porous media were determined from the pressure drop through the microporous media calculated using the CFD program FLUENT 6.1.

A fully numerical simulation of the Navier-Stokes equations for the fluid flow in a porous media with all the particles is very difficult due to the huge number of calculations. Therefore, the present paper considers only a limited number of identical particles as the

porous media. The physical model and the coordinate system are shown in Fig. 1. The calculational region includes an entrance region and an exit region each five d_p long. To simplify the numerical calculations, the packed bed formed by the homogeneous, uniform solid particles was assumed to be periodic in the width direction. The nominal particle sizes of the sintered porous channel were 200 μm, 125 μm, 90 μm, 40 μm, 20 μm and 10 μm. These uniform solid particles were assumed to have small but finite contact areas with a simple cubic lattice structure. Different porosities were obtained by changing the particle sizes and arrangements. Constant thermophysical properties at 290 K were assumed for the air. Periodic boundary conditions were imposed on the boundaries of the computational domain. The inflow into the domain was set as a velocity inlet with the outflow set as the pressure outlet boundary condition.

The dimensions and porosities of the microporous media used in the calculations which were based on the experimental research are listed in Table 1. The constant contact areas between the particles were calculated based on the desired porosity. The numerical simulations used two half particles in the x and y directions with five particles in the z direction for the $d_p = 200$ μm particles, eight particles in the z direction for the $d_p = 125$ μm particles, and 11 particles in the z direction for the $d_p = 90$ μm, $d_p = 40$ μm, $d_p = 20$ μm, and $d_p = 10$ μm particles.

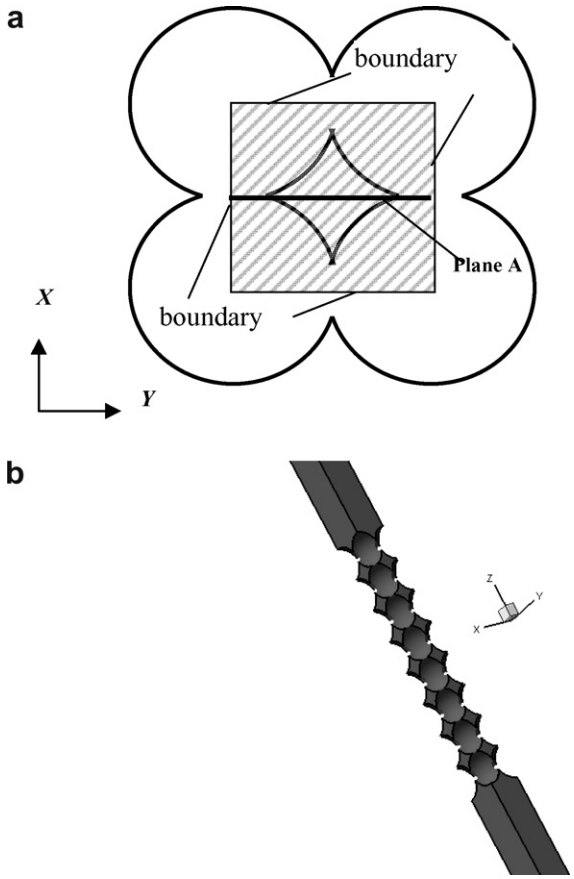

Fig. 1. Schematic diagram of the computational domain.

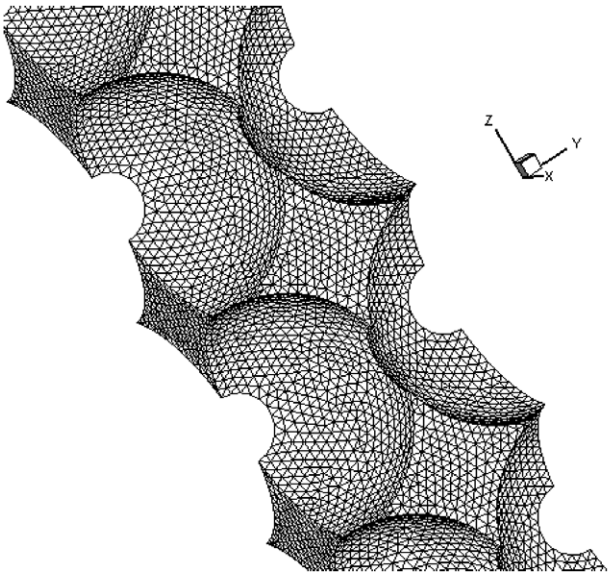

Fig. 2. Surface elements for the computational domain in the test section.

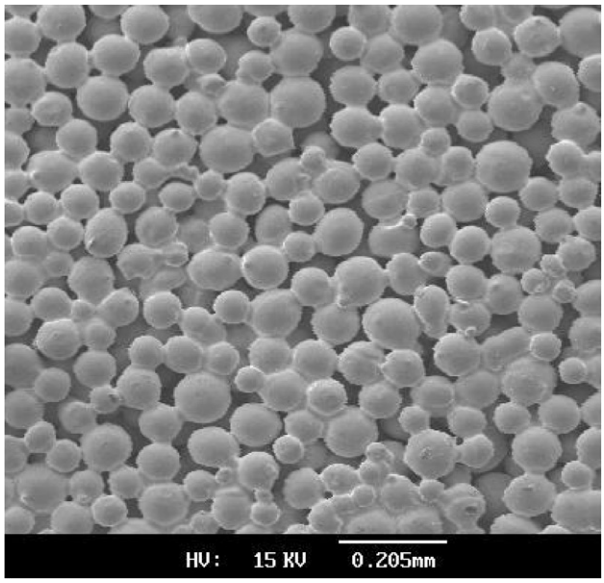

Fig. 3. SEM photograph of the 90 μm average particle diameter microporous media.

Table 1
Geometry and mesh parameters

Test section	Particle diameter d_p (μm)	Porous media length L (mm)	Porosity ε	Total number of elements
No. 1	200	0.980	0.44	779288
No. 2	125	0.978	0.44	857335
No. 3	90	0.970	0.44	1,024,854
No. 4	40	0.416	0.38	1065623
No. 5	20	0.21	0.38	1122425
No. 6	10	0.10	0.34	1097191

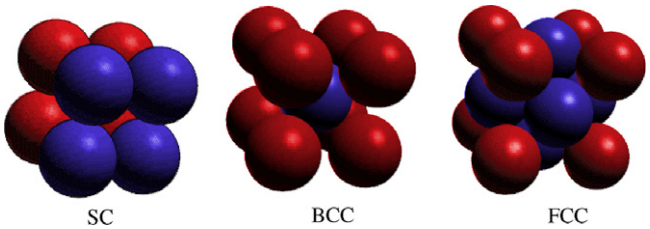

Fig. 4. Arrangements of the particles.

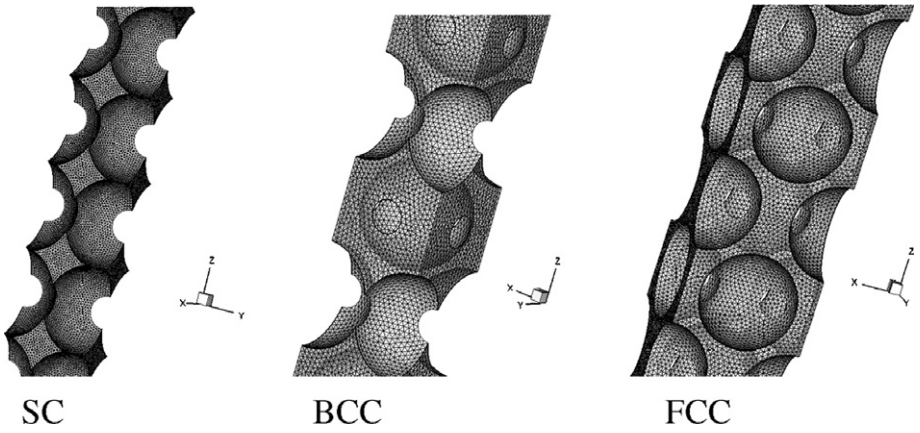

Fig. 5. Meshes for the solid domain for the various particle arrangements.

The FLUENT 6.1 code uses the finite volume method approach with the SIMPLE velocity-pressure coupling algorithm and second-order discretization for the advection terms. The calculations assumed that the air flow was three-dimensional, laminar and incompressible due to the short calculational region. The friction factors were calculated numerically for the non-slip flow and slip flow regimes.

The general equations governing the flow fields for these conditions are: Continuity equation:

$$\frac{\partial u}{\partial x}+\frac{\partial v}{\partial y}+\frac{\partial w}{\partial z}=0 \tag{1}$$

Momentum equations:

$$\rho\left(u\frac{\partial u}{\partial x}+v\frac{\partial u}{\partial y}+w\frac{\partial u}{\partial z}\right)=\frac{\partial P}{\partial x}+\mu\left(\frac{\partial^2 u}{\partial x^2}+\frac{\partial^2 u}{\partial y^2}+\frac{\partial^2 u}{\partial z^2}\right) \tag{2}$$

$$\rho\left(u\frac{\partial v}{\partial x}+v\frac{\partial v}{\partial y}+w\frac{\partial v}{\partial z}\right)=\frac{\partial P}{\partial y}+\mu\left(\frac{\partial^2 v}{\partial x^2}+\frac{\partial^2 v}{\partial y^2}+\frac{\partial^2 v}{\partial z^2}\right) \tag{3}$$

$$\rho\left(u\frac{\partial w}{\partial x}+v\frac{\partial w}{\partial y}+w\frac{\partial w}{\partial z}\right)=\frac{\partial P}{\partial z}+\mu\left(\frac{\partial^2 w}{\partial x^2}+\frac{\partial^2 w}{\partial y^2}+\frac{\partial^2 w}{\partial z^2}\right) \tag{4}$$

For the slip flow regime, the additional boundary conditions to model the slip flow are:

$$U_w-U_g=-\left(\frac{2-\alpha_v}{\alpha_v}\right)Kn\frac{\partial U}{\partial n}\approx\left(\frac{2-\alpha_v}{\alpha_v}\right)\frac{l}{\delta}(U_g-U_c) \tag{5}$$

$$V_g\equiv\left(\vec{V}\cdot\vec{n}\right)_g=V_w \tag{6}$$

$$l=\frac{k_B T}{\sqrt{2}\pi\sigma^2 p} \tag{7}$$

Where U and V represent the non-dimensional velocity components parallel and normal to the wall, respectively. n is the wall normal

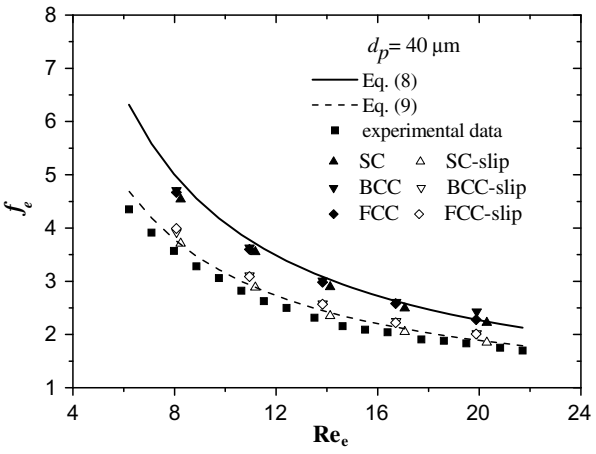

Fig. 6. Comparison of the calculated results for f_e for the SC, BCC and FCC particle arrangements with Eqs. (8) and (9) and experimental data.

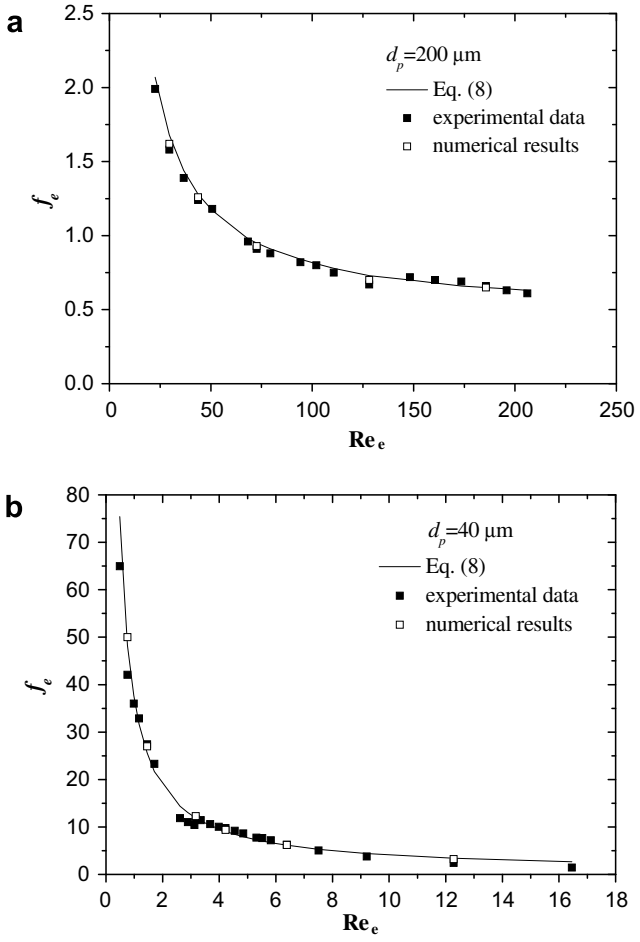

Fig. 7. Comparison of numerically predicted friction factors for water with experimental data and predictions of Eq. (8).

coordinate normalized by the pore diameter. The subscripts g, w and c indicate the gas, wall and cell-center velocities. l is the average molecular free path. δ is the distance from the cell-center to the wall. α_v is the momentum accommodation coefficient of the gas which was set to 0.6 for this study.

The grid independence was first examined to minimize the numerical uncertainties. Because of the limited computer memory, a simpler example was run using a calculational region including an entrance region and an exit region with lengths of 3 d_p. A mesh refinement study was used to examine the effects of the mesh density on the solution with three kinds of mesh size. Each particle had either 600, 800 or 1000 nodes on the surface with 3000, 4000 or 5000 elements on the surface. The spaces between adjacent particles had from 400 to 600 nodes. The numerical results using the mesh with 800 nodes on each particle surface and 500 nodes in the spaces between adjacent particles were approximately 4% higher for $\triangle P$ compared to the mesh with 600 nodes on each particle surface and 400 nodes in the spaces between adjacent particles and approximately 0.9% lower for $\triangle P$ compared to the mesh with 1000 nodes on each particle surface and 600 nodes in the spaces between adjacent particles. The mesh with 800–1000 nodes on each particle surface and 500–600 nodes in the spaces between

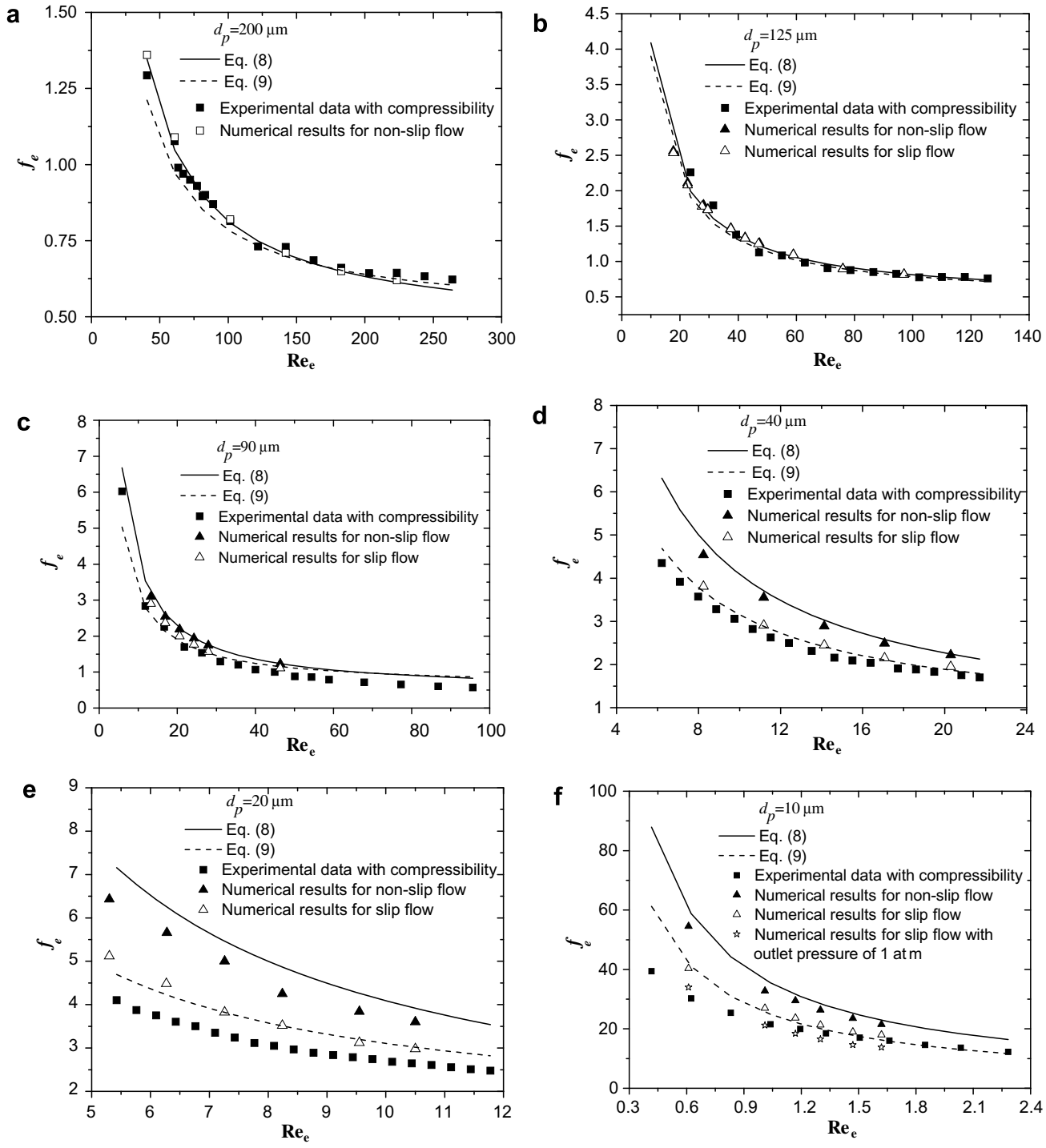

Fig. 8. Comparison of numerically predicted friction factors with experimental data and predictions of Eq. (8).

adjacent particles was, therefore, deemed acceptable. However, for the whole calculational region including entrance and exit regions each with lengths of 8 d_p, the mesh with 1000 nodes on each particle surface resulted in a very large number of nodes that exceeded the computer memory. Therefore, the mesh with 800 nodes on each particle surface and 500 nodes in the spaces between adjacent particles is used in the following calculations.

An example mesh for the solid domain is shown in Fig. 2. Table 1 lists the geometry and mesh parameters used for each case to give the best computational accuracy within the constraints of the available computational resources. The convergence criteria were 10^{-8} for each velocity component as well as for pressure. The results described in the next section show that this element density gave accurate results.

3. Influence of the particle arrangement on the fluid flow in micro porous media

The actual porous structure in the porous media is usually not as regular or uniform as shown in Fig. 3. The influence of the particle arrangement on the fluid flow in the micro porous media was investigated using three different particle arrangements, simple cubic (SC), body centered cubic (BCC) and face centered cubic (FCC) geometries as shown in Fig. 4. The calculational models and meshes for the different particle arrangements (SC, BCC and FCC) are shown in Fig. 5.

Xu et al. (2008) showed that the measured friction factors for air in the porous media with average diameters of 200 μm and 125 μm with consideration of compressibility agree well with the following correlation for normal size porous media:

$$f_e = \frac{\varepsilon^3}{1-\varepsilon}\frac{\rho d_p}{3M^2}\frac{\Delta P}{L} = \frac{36.4}{\mathrm{Re}_e} + 0.45 \quad (\text{for } \mathrm{Re}_e < 2000) \tag{8}$$

However, the measured friction factors for air in the porous media with average diameters of 10 μm–90 μm with consideration of compressibility were less than the correlation in Eq. (8), so Eq. (8) was modified to account for the compressibility and rarefaction effects (Xu et al., 2008):

$$f_e = \frac{36.4}{\mathrm{Re}_e(1+443\overline{\mathrm{Kn}})} + 0.45\cdot\frac{(1+3.39\times10^5\cdot\overline{\mathrm{Kn}}^{1.9})}{(1+443\overline{\mathrm{Kn}})^{1/2}} \tag{9}$$

Fig. 6 compares the calculated results for f_e for the SC, BCC and FCC arrangements of the particles with Eqs. (8) and (9) and experimental data for d_p = 40 μm for various Re_e. The solid symbols are the calculated results using the SC, BCC and FCC arrangements of the particles without consideration of velocity slip on the solid wall, while the hollow symbols are the calculated results using the SC, BCC and FCC arrangements of the particles with consideration of velocity slip on the solid wall. The results show that the differences between the numerical results using the SC, BCC and FCC arrangements of the particles without consideration of velocity slip on the solid wall and the results using Eq. (8) were less than 6.7%, 6.6% and 5.9%, respectively. The good agreement confirms again that the particle-level numerical simulations can properly simulate the fluid flow in porous media for flows without rarefaction as shown in Jiang and Lu (2006a). The differences between the numerical results using the SC, BCC and FCC arrangements of the particles with consideration of the velocity slip on the solid wall and the experimental data and Eq. (9) were less than 5%, 10% and 11% for the three arrangements. The particle arrangements in the porous media influence the fluid flow for flows with velocity slip on the wall due to the different surface areas in the different arrangements. However, these differences are not large; thus, the SC particle arrangement was used for the following numerical simulations.

4. Numerical results and discussion

4.1. Friction factor of water and air in micro porous media

Fig. 7 compares the numerical results for the friction factor of water with previous experimental data (Xu et al., 2008) and the predictions of Eq. (8). The results show that the numerically predicted friction factors of water without consideration of velocity slip on the wall in the microporous media agree well with Eq. (8) and the experimental data. These results confirm that the numerical simulations are reliable and there is no abnormal phenomenon for water flow in the microporous media.

Fig. 8 compares the numerically predicted friction factors for air with experimental data and the predictions of Eqs. (8) and (9). The results show that for all the test sections the numerically predicted friction factors for non-slip flow in the microporous media agree

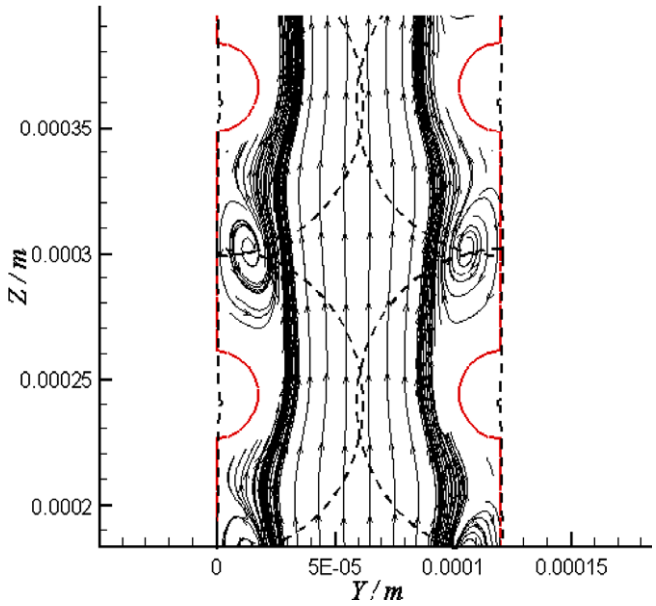

Fig. 9. Streamlines for air flow in plane *A* in microporous media with d_p = 125 μm.

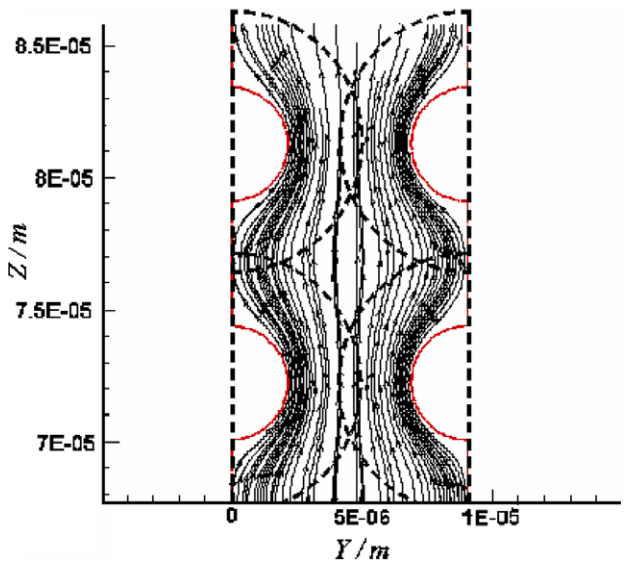

Fig. 10. Streamlines for air flow in plane *A* in microporous media with d_p = 10 μm.

well with Eq. (8), which confirms again that the numerical simulations are reliable for air flow in porous media.

Test section No. 1 with d_p = 200 μm had an average pore diameter of about 110 μm and an average Knudsen number for air of 0.64×10^{-3}. Therefore, for this condition, the velocity slip can be ignored as shown by the numerical results without consideration of velocity slip on the wall which agree well the experimental data and the predictions of Eqs. (8) and (9) as shown in Fig. 8a. Test section No. 2 had an average pore diameter of about 68 μm and Knudsen numbers of 6×10^{-4}–9×10^{-4} for the air flow tests. The results in Fig. 8b shows that the rarefaction again had very little influence on the fluid flow in the microporous media for d_p = 125 μm.

Test section No. 3 with d_p = 90 μm had an average pore diameter of about 49 μm and Knudsen numbers of 0.7×10^{-3}–1.3×10^{-3} for the air flow tests. For these conditions, the rarefaction had a slight influence on the air flow in the microporous media as shown by the good agreement between the numerical results with consideration of velocity slip on the wall and the experimental data and the values predicted by Eq. (9) shown in Fig. 8c. Test sections No. 4–6 had average pore diameters of about 16 μm, 8.2 μm and 3.4 μm, and Knudsen numbers of 2.9×10^{-3}–3.7×10^{-3}, 3.7×10^{-3}–5.3×10^{-3} and 3.5×10^{-3}–$10 \times 10^{-3}$for the air flow tests. The numerical simulations show that the differences between the non-slip flow and slip flow results increases with decreasing average particle diameter (Fig. 8d–f). The numerical results for the friction factor without consideration of velocity slip on the wall agreeing well with the values predicted by Eq. (8), but the numerically predicted slip flow friction factors in the microporous media with average particle diameters of 40 μm, 20 μm and 10 μm are less than the values predicted by Eq. (8), but close to the experimental results and the values predicted by Eq. (9). Therefore, these results further illustrate the micro-scale and rarefaction effects in the microporous media with $d_p \leqslant 90$ μm. In addition, Fig. 8d–f show that the differences between the numerically predicted friction factors with and without consideration of the slip flow decrease as the velocity increases. This can be attributed to the variation of the mean free path of air with pressure (Xu et al., 2008).

Fig. 8f also illustrates the influence of the outlet pressure in the numerical simulations which affects the mean free path of the air in the microporous media. For the same microporous media and air velocity, the calculated friction factors with an outlet pressure of 1 atm are less than these with an outlet pressure equal to the average of the inlet and outlet pressures in the real experiments

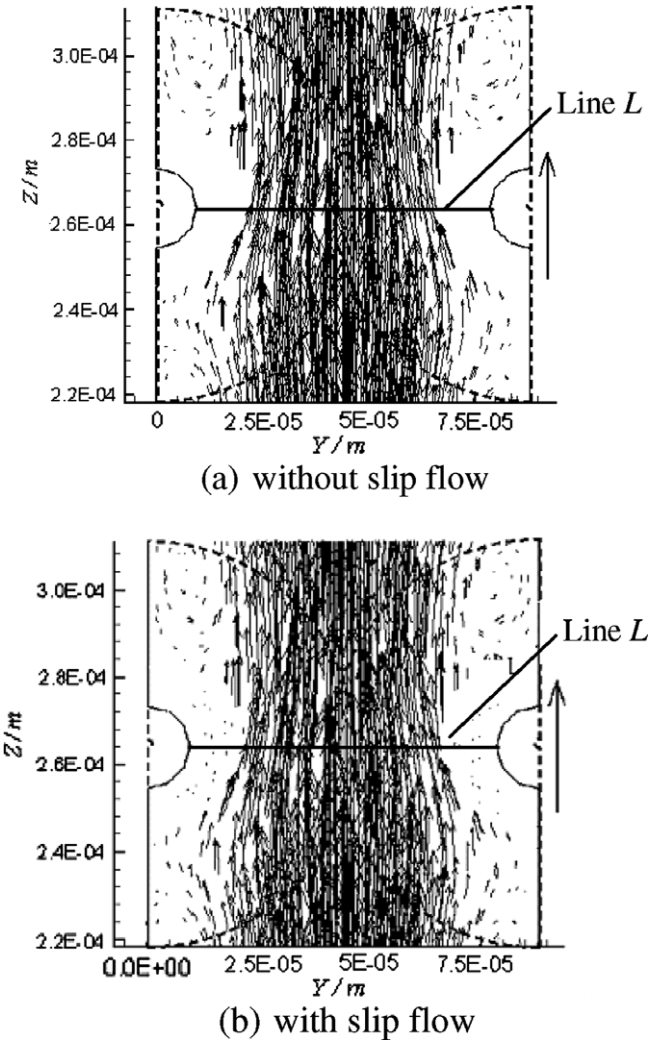

Fig. 11. Air velocity vectors in test section No. 3 with d_p = 90 μm, u_0 = 2.8 m/s, and $\overline{Kn}$ = 0.0011 for both non-slip and slip flow conditions.

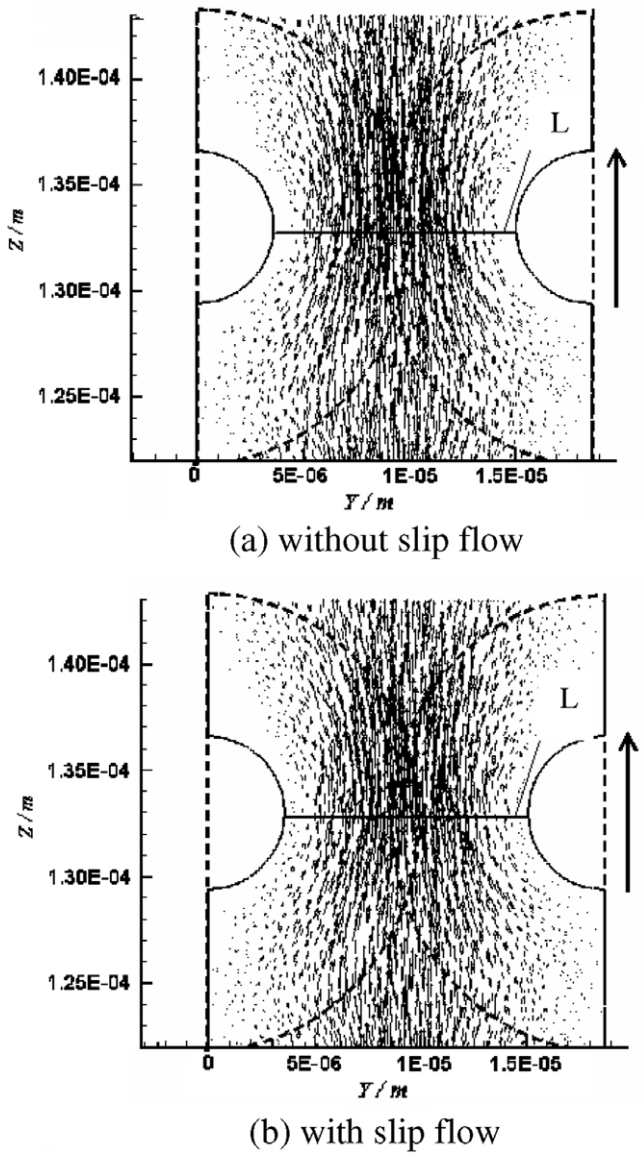

Fig. 12. Air velocity vectors in test section No. 3 with d_p = 20 μm, u_0 = 2.8 m/s, and $\overline{Kn}$ = 0.0058 for both non-slip and slip flow conditions.

because the mean free path of air in the porous media decreases with increasing pressure which reduces the Knudsen number. The differences between the calculated friction factors with the two different outlet pressures are about 18% for the lower flow rates and 23% for the larger flow rates.

For test sections No. 5–6 with d_p = 20 μm and 10 μm, the calculated friction factors are still larger than the experimental data (Xu et al., 2008), which needs study further.

4.2. Streamlines and velocity distributions in the micro porous media

Fig. 1a shows the typical geometries and flow units used in the calculations. The streamlines and velocity vectors in plane *A* in Fig. 1a are described in this section.

Fig. 9 shows the streamlines for air flow in plane *A* in the microporous media with d_p = 125 μm for the 1.8 m/s inlet velocity. The trends are similar for the other velocities in all the test sections. The results show that the microporous structure creates substantial mixing and vortex shedding which increase the friction factor. The vortex shedding occurs near the contact points along the flow direction.

Fig. 10 shows the streamlines for air flow in plane *A* in the microporous media with d_p = 10 μm for the 1.88 m/s inlet velocity. The smaller particles and smaller porosity do not create vortices in the flow, which differs from the air flow in plane *A* for d_p = 125 μm.

Figs. 11 and 12 show the air velocity vectors in test section No. 3 with d_p = 90 μm for the 2.8 m/s inlet velocity and in test section No. 5 with d_p = 20 μm for the 2.8 m/s inlet velocity for both the non-slip and slip flow cases. The results using the same reference vector length show that the velocity slip near the wall is quite noticeable. In addition, the maximum velocities are 10 times the inlet velocity in the restricted flow areas in the microporous media.

The velocity distributions along line *L* shown in Figs. 11 and 12 in test sections No. 3 and No. 5 are shown in Fig. 13 for both the slip and non-slip cases for the same Reynolds number. As expected, the velocity slip increases as the Knudsen number increases. For the microporous media with d_p = 20 μm, the velocity increase near the wall and the velocity decrease in the channel center due to the slip flow are more evident than for d_p = 90 μm.

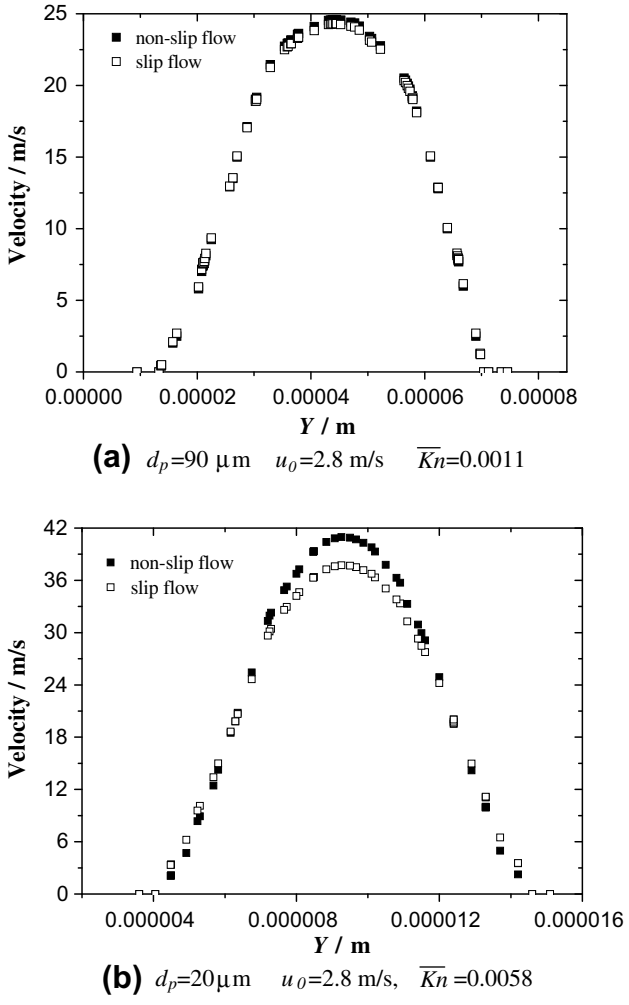

Fig. 13. Velocity distributions along line *L* in the microporous media.

5. Conclusions

The flow characteristics of water and air in microporous media were investigated numerically using the CFD code FLUENT. The results show that:

An investigation of the influence of the particle arrangement on the fluid flow in micro porous media showed that the simple cubic arrangement of particles is suitable for the numerical simulations.

The friction factors calculated for the non-slip flow regime in the microporous media agree well with the correlation for normal scale porous media.

The numerically predicted friction factors using the slip flow boundary condition in the microporous media with average particle diameters of 90–10 μm were less than the non-slip flow correlation but close to the experimental results and the values predicted by the modified correlation with consideration of compressibility and rarefaction.

Comparisons of the experimental and numerical results with standard correlations show that rarefaction occurs in air flows in the microporous media with particle diameters less than 90 μm and that the numerical calculations with velocity slip on the boundary can properly simulate the slip flows in microporous media.

Acknowledgement

This project was supported by the Key Project Fund from the National Natural Science Foundation of China (No. 50736003) and the National Basic Research Program (973 Program) (No. 2007CB210107).

References

Aerov, M.E., Tojec, O.M., 1968. Hydraulic and thermal basis on the performance of apparatus with stationary and boiling granular layer. Leningrad, Himia Press, in Russian.

Alazmi, B., Vafai, K., 2002. Constant wall heat flux boundary conditions in porous media under local thermal non-equilibrium conditions. International Journal of Heat and Mass Transfer 45, 3071–3087.

Amiri, A., Vafai, K., Kuzay, T.M., 1995. Effects of boundary conditions on non-Darcian heat transfer through porous media and experimental comparisons. Numerical Heat Transfer, Part A 27, 651–664.

Antohe, B.V., Lage, J.L., Price, D.C., Weber, R.M., 1997. Experimental determination of permeability and inertia coefficients of mechanically compressed aluminum porous matrices. Journal of Fluids Engineering 119, 404–412.

Bravo, M.C., 2007. Effect of transition from slip to free molecular flow on gas transport in porous media. Journal of Applied Physics 102, 074905.

Eckert, E.G.R., Drake, R.M., 1972. Analysis of Heat and Mass Transfer. McGraw-Hill. pp. 467–486.

Ergun, S., 1952. Fluid flow through packed columns. Chemical Engineering Progress 48, 89–94.

Ertekin, T., King, G.R., Schwerer, F.C., 1986. Dynamic gas slippage: a unique dual-mechanism approach to the flow of gas in tight formations. SPE Formation Evaluation 1, 43–52.

Guardo, A., Coussirat, M., Larrayoz, M., 2005. Influence of the turbulence model in CFD modeling of wall-to-fluid heat transfer in packed beds. Chemical Engineering Science 60, 1733–1742.

Hsu, C.T., Cheng, P., 1990. Thermal dispersion in a porous medium. International Journal of Heat and Mass Transfer 33, 1587–1597.

Jiang, P.X., Ren, Z.P., Wang, B.X., 1999a. Numerical simulation of forced convection heat transfer in porous plate channels using thermal equilibrium and nonthermal equilibrium models. Numerical Heat Transfer, Part A 35, 99–113.

Jiang, P.X., Wang, Z., Ren, Z.P., Wang, B.X., 1999b. Experimental research of fluid flow and convection heat transfer in porous plate channels filled with glass or metallic particles. Experimental Thermal Fluid Science 20, 45–54.

Jiang, P.X., Ren, Z.P., 2001. Numerical investigation of forced convection heat transfer in porous media using a thermal non-equilibrium model. International Journal of Heat and Fluid Flow 22 (1), 102–110.

Jiang, P.X., Li, M., Ma, Y.C., Ren, Z.P., 2004. Boundary conditions and wall effect for forced convection heat transfer in sintered porous plate channels. International Journal of Heat and Mass Transfer 47, 2073–2083.

Jiang, P.X., Lu, X.C., 2006a. Numerical simulation of fluid flow and convection heat transfer in sintered porous plate channels. International Journal of Heat and Mass Transfer 49 (9–10), 1685–1695.

Jiang, P.X., Xu, R.N., Gong, W., 2006b. Particle-to-fluid heat transfer coefficients in miniporous media. Chemical Engineering Science 61 (2), 7213–7222.

Jones, F.O., Owens, W.W., 1980. A laboratory study of low-permeability gas sands. Journal of Petroleum Technology 32, 1631–1640.

Klinkenberg, L.J., 1941. The Permeability of Porous Media to Liquids and Gas. Drilling and Productions Practices. American Petroleum Institute. pp. 200–213.

Liu, J.Q., Tai, Y.C., Ho, C.M., 1995. MEMS for pressure distribution studies of gaseous flows in microchannels. In: Proceedings, IEEE Micro Electro Mechanical Systems, pp. 209–215.

Logtenberg, S.A., Nijemeisland, M., Dixon, A.G., 1999. Computational fluid dynamics simulations of fluid flow and heat transfer at the wall-particle contact points in a fixed-bed reactor. Chemical Engineering Science 54, 2433–2439.

Kast, W., Hohenthanner, C.R., 2000. Mass transfer within the gas-phase of porous media. International Journal of Heat and Mass Transfer 43, 807–823.

Ma, W.P., Tzeng, S.C., Jwo, W.J., 2006. Flow resistance and forced convective heat transfer effects for various flow orientations in a packed channel. International Communications in Heat and Mass Transfer 33, 319–326.

Magnico, P., 2003. Hydrodynamic and transport properties of packed beds in small tube-to-sphere diameter ratio: pore scale simulation using an Eulerian and a Lagrangian approach. Chemical Engineering Science 58, 5005–5024.

Maurer, J., Tabeling, P., Joseph, P., Willaime, H., 2003. Second-order slip laws in microchannels for Helium and Nitrogen. Physics of Fluids 15, 2613–2621.

Miguel, A.F., Serrenho, A., 2007. On the experimental evaluation of permeability in porous media using a gas flow method. Journal of Physics D: Applied Physics 40, 6824–6828.

Nijemeisland, M., Dixon, A.G., 2001. Comparison of CFD simulations to experiment for convective heat transfer in a gas–solid fixed bed. Chemical Engineering Journal 82, 231–246.

Nijemeislanda, M., Dixon, A.G., Stittb, E.H., 2004. Catalyst design by CFD for heat transfer and reaction in steam reforming. Chemical Engineering Science 59, 5185–5191.

Pavan, V., Oxarango, L.J., 2007. A new momentum equation for gas flow in porous media: the Klinkenberg effect seen through the kinetic theory. Journal of Statistical Physics 126 (2), 355–389.

Polyaev, V.M., Mozhaev, A.P., Galitseysky, B.M., Lozhkin, A.L., 1996. A study of internal heat transfer in nonuniform porous structures. Experimental Thermal and Fluid Science 12, 426–432.

Quintard, M., 1998. Modeling local non-equilibrium heat transfer in porous media. Heat Transfer 1998, In: Proceedings 11th International Heat Transfer Conference, Kyongju, Korea, 1, pp. 279–285.

Sampath, K., Keighin, C.W., 1982. Factors affecting gas slippage in tight sandstones of cretaceous age in the Uinta basin. Journal of Petroleum Technology 34, 2715–2720.

Scheidegger, A.E., 1974. The physics of flow through porous media. Third ed. University of Toronto Press.

Tzeng, S.C., Jeng, T.M., Wang, Y.C., 2006. Experimental study of forced convection in asymmetrically heated sintered porous channels with/without periodic baffles. International Journal of Heat and Mass Transfer 49, 78–88.

Vafai, K., Tien, C.L., 1981. Boundary and inertial effects on flow and heat transfer in porous media. International Journal of Heat and Mass Transfer 24, 195–203.

Wakao, N., Kaguei, S., 1982. Heat and Mass Transfer in Packed Beds. Gordon and Breach, New York.

Xu, R.N., Jiang, P.X., Huang, Y.L. Zhao, C.R., 2008. Flow Characteristics through Microporous Media. submitted to International Journal of Heat and Fluid Flow.